THE AMERICAN SOCIETY OF MECHANICAL ENGINEERS
345 E. 47th St., New York, N.Y. 10017

94-GT-461

UNSTEADY ENDWALL/TIP-CLEARANCE FLOWS AND LOSSES DUE TO TURBINE ROTOR-STATOR INTERACTION

Atsumasa Yamamoto
Aeroengine Division
National Aerospace Laboratory
Tokyo, Japan

Takayuki Matsunuma, Kenichiro Ikeuchi,[1] and Eisuke Outa
Department of Mechanical Engineering
Waseda University
Tokyo, Japan

ABSTRACT

Unsteady static pressure on the tip endwall of a 1.5-stage low-speed axial-flow turbine was measured in detail using a micro high-response pressure transducer to investigate effects of rotor-stator interaction on the endwall and tip-clearance flows which play important roles in turbine loss generation process. In the present paper, distributions of the time-averaged and the time-dependent pressures over the first-stage rotor and the second-stage stator are presented. Also time-averaged and time-dependent random fluctuations of the pressure were analyzed to understand unsteady behaviors of the flows and the associated losses over the endwall as well as inside the blade tip clearance. These unsteady characteristics were described for three rotor speeds with different incidences or loadings. Significantly large random fluctuations occur around the blade surfaces, particularly at the inlet and the outlet of the tip gap of the leakage flows, and in a flow separated region from the blade leading edge in a large negative incidence case. A strong relation was found between the random fluctuation of the endwall static pressure and the total pressure loss inside the rotor, where large random fluctuation is attributed to high loss and vice versa. It can be seen clearly that the loss generation process is fairly unsteady due to the rotor-stator interaction.

NOMENCLATURE

Cax = blade axial chord
CPs = static pressure coefficient
CPt = total pressure coefficient
CPw = endwall static pressure coefficient
F = free stream
H = passage height
i = incidence
LFp, LFs = large random fluctuation area at blade pressure or suction side
LPG = large pressure gradient region
PV = passage vortex
ST = stagnation area of inlet endwall flow around blade leading edge
i = number of axial traverse measuring points
j = number of circumferential traverse measuring points
n = number of phase-locked data
t = number of instantaneous time steps
T = rotor passing period
TV = tip leakage vortex
U = circumferential speed of rotor
Vax = axial flow velocity
W = wake
Y = spanwise distance from hub endwall
Z = axial distance from rotor leading edge
Δ[ ] = interval of contour plots

(subscripts)

1 = rotor inlet
ax = axial
hub = hub side
mid = midspan
p, s = blade pressure side or suction side
tip = tip side
~ = phase-locked average

[1] Current address: Japan Airlines Co. Ltd., Narita, Chiba

Presented at the International Gas Turbine and Aeroengine Congress and Exposition
The Hague, Netherlands — June 13–16, 1994

$\bar{}$ = time-averaged value in a rotor passing period

$'$ = random fluctuation of endwall static pressure

INTRODUCTION

The losses associated with the endwall boundary layer flow and the leakage flow through the blade tip clearance dominate a large part of the overall loss in turbine blade rows. It is, therefore, necessary to reveal the loss generation process near the endwall as well as in the tip clearance in order to improve the turbine performance further. A lot of detailed experimental studies have been carried out, for example, on mechanisms of leakage flows within blade tip gaps (Bindon, 1986,1988; Moore and Tilton, 1987), on effects of the incidence, tip clearance size and tip geometry on the endwall/tip-clearance loss generation (Yamamoto, 1989; Heyes, et al., 1991), on effects of casing wall movement on tip leakage flow (Yaras and Sjolander, 1991) etc. All of these studies have been done with stationary cascades. Internal flows of actual turbines, however, exhibit extremely complex unsteady flows due to the interaction between the rotational and the stationary blade rows. Therefore, the endwall flows close to the endwall and within the tip clearance, which are important to see the loss generation process, are considered to be strongly influenced by the interaction.

In the present study, unsteady static pressures on the rotor and stator tip endwall were measured using a micro high-response pressure transducer. Results are presented for three different rotor speeds with a constant turbine mass flow rate, which correspond to three different blade loading conditions with different incidences. To understand complex behaviors of the unsteady endwall flows over the rotor and the stator clearly, the unsteady endwall pressures obtained are divided into the time-averaged pressure (periodic fluctuation part) and the random fluctuation of the pressure. The random fluctuation was compared to total pressure loss inside the rotor passage, and a strong relation between the random fluctuation and the total pressure loss was found to exist.

EXPERIMENTAL METHOD AND ANALYSIS METHOD

Experiments was made with a NAL 1.5-stage, low-speed, axial-flow turbine, as shown in Fig.1. The first stage stator was located far enough from the rotor to attain a circumferentially uniform swirling flow into the rotor without strong circumferential wake deficits coming from the upstream stator. The measurements were made over the tip casing covering the first stage rotor and the second stage stator, as shown in Fig.1 as a measuring window. The rotor has a tip clearance of 1.2mm which corresponds to 1.6 percent of the rotor passage height. A tip clearance of 0.8mm (corresponding to 1.2 percent of the stator passage height) was also left in the downstream stator intentionally to see effects of the upstream cascade movement on the downstream cascade tip leakage flow. The major specifications of the test first-stage rotor and second-stage stator

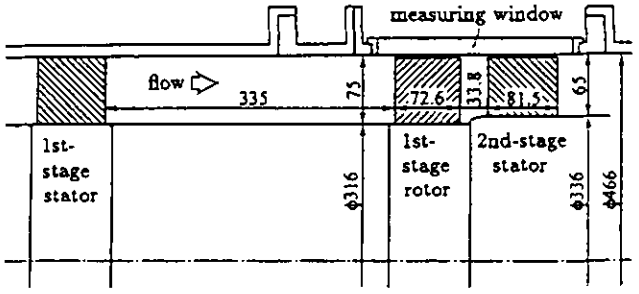

Fig.1 Schematic drawing of test turbine

Table.1 Major specifications of test cascades

		First rotor	Second stator
Blade number	N	20	16
Blade chord	C	73.5 mm	104.4 mm
Blade axial chord	Cax	72.6 mm	81.5 mm
Blade span (passage height)	H	75.0 mm	65.0 mm
Blade pitch at midspan	S	61.42 mm	78.74 mm
Blade inlet camber angle	α in	-49.8 deg	0.0 deg
Blade outlet camber angle	α out	63.5 deg	-68.0 deg
Blade turning angle	$\Delta\alpha$	113.3 deg	68.0 deg
Design inlet flow angle	θ y, in	-43.6 deg	0.0 deg
Design outlet flow angle	θ y, out	63.5 deg	-68.8 deg
Design flow turning angle	$\Delta\theta$ y	107.1 deg	68.0 deg
Cascade stagger angle	ξ	-17.2 deg	-39.0 deg
Cascade aspect ratio	H/C	1.020	0.623
Cascade solidity	C/S	1.20	1.33
Leading-edge thickness ratio	D(LE)/C	0.111	0.127
Trailing-edge thickness ratio	D(TE)/C	0.056	0.033
Blade max. thickness ratio	Dmax/C	0.257	0.211
Hub/Tip diameter	Dtip/Dbub	316/466 mm	336/466 mm

are shown in Table.1. Further details on the test turbine may be found in some previous papers (e.g., Yamamoto et al., 1993).

Fig.2 shows (a) a micro high-response pressure transducer (the head diameter is 1.63mm and the natural frequency is 100 KHz), (b) details of the transducer adapters, and (c) relative locations among the cascades, totally 22 axial measurement holes (i=22) into which the adapters are inserted, and nine circumferential measuring points (j=9). The transducer output was sensitive to its surrounding temperature change, while the output linearity was not, and therefore, the output data was used to detect only periodically unsteady pressure deviated from its time averaged value and the random fluctuation of the pressure. The overall unsteady pressure at each measuring point was then obtained by adding the periodically unsteady pressure to 'steady' pressure obtained at the same measuring point. The 'steady' pressure was separately obtained by usual steady state measurements with a pressure transducer of larger size with better temperature compensation circuit.

Fig.3 shows the present measuring system used. Pressure data from the micro pressure transducer were taken into a high-speed digital transient memory (the maximum sampling speed is 1

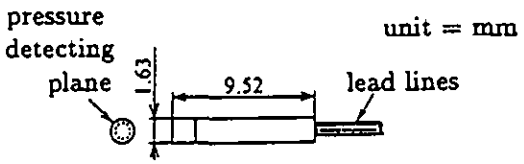

(a) micro pressure transducer

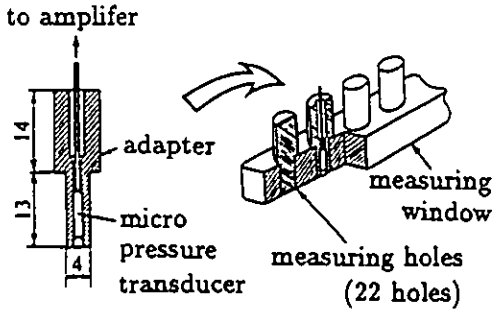

(b) details of transducer adapters

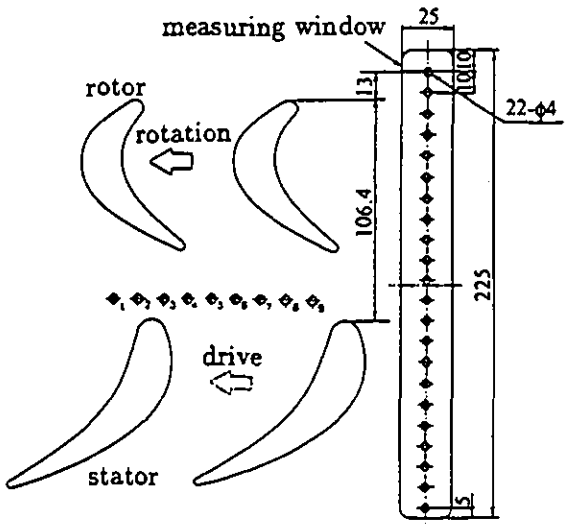

(c) relative locations between measuring points and cascades

Fig.2 Measuring section

MHz) with synchronizing the data sampling with the pulses (400 pulses per rotor revolution or 20 pulses per rotor blade pitch; t=20) coming from an encoder connected to the rotor axis. The circumferential positions of the sensor with respect to the stator were changed nine times (j=9) by driving the stator in the pitchwise direction as shown by a dotted arrow in Fig.2(c). Totally 408 phase-locked (n=408) pressure data (Pm) at each measuring point ($i \times j$ =22 axial × 9 circumferential) were obtained, and are averaged to get the (mean) periodic fluctuation ($\widetilde{Pm}$). The random fluctuation ($\widetilde{Pm}'$) deviated from $\widetilde{Pm}$ was then obtained. These were nondimensionalized by the following

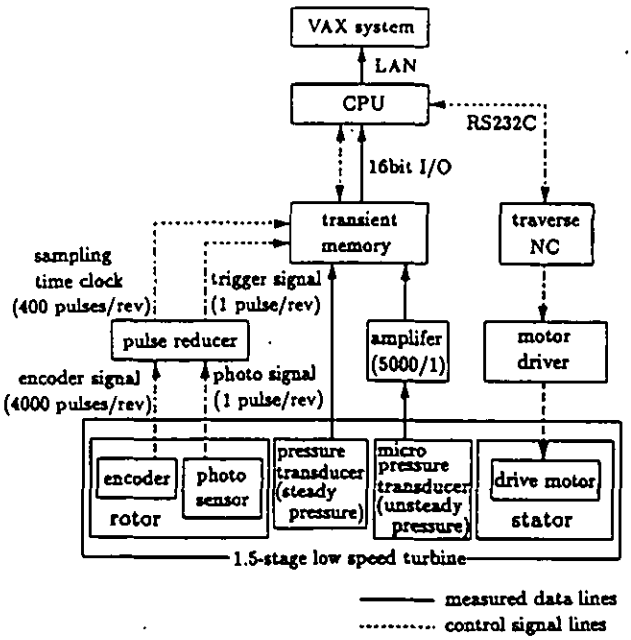

Fig.3 Measuring system

formulae:

$$CPw_{(i,j,t)} = \frac{\widetilde{Pm}_{(i,j,t)} - P_{1,w}}{\frac{1}{2}\rho \cdot V_{1,mid}{}^2} \quad \text{(periodic fluctuation coefficient)}$$

$$CPw'_{(i,j,t)} = \frac{\widetilde{Pm}'_{(i,j,t)}}{\frac{1}{2}\rho \cdot V_{1,mid}{}^2} \quad \text{(random fluctuation coefficient)}$$

$$\text{where } \widetilde{Pm}_{(i,j,t)} = \sum_{n=1}^{408} Pm_{(i,j,t,n)} \Big/ 408$$

(phase-locked averaged pressure)

$$\widetilde{Pm}'_{(i,j,t)} = \sqrt{\sum_{n=1}^{408} (Pm_{(i,j,t,n)} - \widetilde{Pm}_{(i,j,t)})^2} \Big/ 408$$

(random fluctuation of pressure)

where $P_{1,w}$ is the pitch-averaged endwall static pressure at the most upstream measuring hole, and $V_{1,mid}$ is the flow velocity at the midspan of the rotor inlet (at Z/Cax = −0.16, i.e., 16% rotor blade axial chord upstream from the rotor leading edge), both obtained in the stationary frame of reference, and ρ is density. The time-average values of the periodic fluctuation, $\overline{CPw}$, and the random fluctuation, $\overline{CPw'}$, are obtained by averaging those at all 'instantaneous time steps' which correspond to different relative locations between the rotor and the stator. With the present measuring technique described above, however, somewhat complicated procedure was necessary to obtain the time-averaged pressure fields of the rotor in the rotational frame of reference and those of the stator in the stationary frame; To

Table.2 Test conditions

(a) ROTOR

	INCIDENCE		
	330rpm	522rpm	760rpm
TIP (Y/H=0.984)	−4.5 deg	−45.2 deg	−98.8 deg
MID (Y/H=0.500)	+2.2 deg	−12.0 deg	−43.7 deg
HUB (Y/H=0.016)	−5.1 deg	−20.7 deg	−49.3 deg
	(Vax/U) mid		
MID (Y/H=0.500)	1.105	0.701	0.481

(b) STATOR

	INCIDENCE		
	330rpm	522rpm	760rpm
TIP (Y/H=0.984)	+18.4 deg	−2.4 deg	−56.0 deg
MID (Y/H=0.500)	+23.5 deg	+22.7 deg	−23.5 deg
HUB (Y/H=0.016)	+50.5 deg	+29.2 deg	−46.1 deg

say simply without explaining the complicated procedure, for the rotor, the number of instantaneous time steps corresponds to j (totally 9 steps), and for the stator, it corresponds to t (totally 20 steps):

$$\overline{CPw_{(i,j)}} = \sum^{9or20} CPw_{(i,j,t)} \Big/ (9or20)$$

$$\overline{CPw'_{(i,j)}} = \sum^{9or20} CPw'_{(i,j,t)} \Big/ (9or20)$$

Tests were carried out for three different rotor speeds with keeping the turbine mass flow rate constant; the test rotor speeds are 330, 522 and 760 rpm which correspond to the rotor incideces at the midspan of +2.2, −12.0 and −43.7 deg, respectively, and also correspond to high, medium and low loading conditions. The −12.0 deg incidence at 522 rpm is closest to the design incidence (−6.2 deg), as can be known from $\alpha_{in}-\theta_{y,in}$ given in Table 1, and in the following discussion, this speed will be referred as the design speed with medium loading. Note that the incidences measured near the blade tip, however, are significantly different from those at the midspan, as shown in Table 2 and later in (a) of Figs.4, 5 and 6. The total pressure and the total temperature of the air in the test section are 1 atmospheric pressure and 15 deg C (the standard atmospheric condition). The test axial Much number is 0.024. Due to this very low speed test condition, the test rig was stable enough to

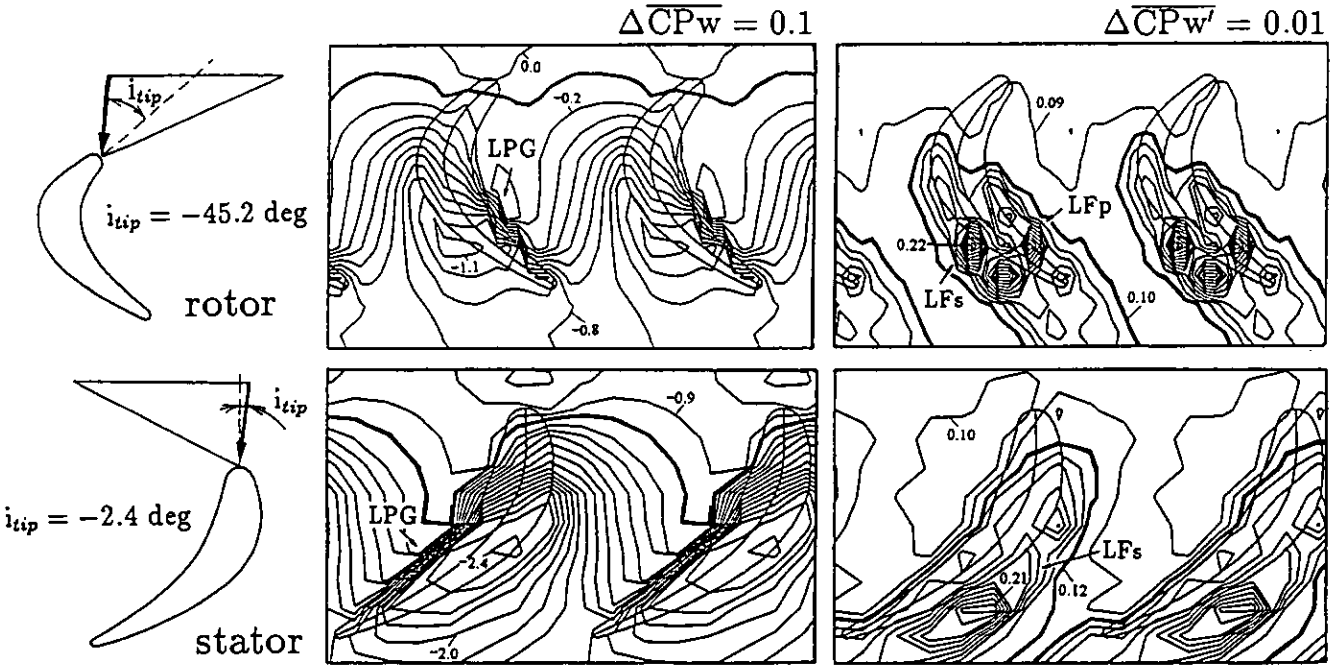

(a) velocity triangle at tip endwall

(b) endwall static pressure $\overline{CPw}$

(c) random fluctuation of endwall static pressure, $\overline{CPw'}$

Fig.4 Time-averaged distributions at medium loading

make accurate unsteady pressure measurements without any vibration problems. Test Re numbers based on the blade chord and the outlet velocity are about 0.9×10^5 for the rotor and 1.5×10^5 for the stator. Detailed test conditions on the incidences of both cascades and the axial/circumferential velocity ratios (Vax/U) at the rotor inlet in the stationary frame are summarized in Table 2.

EXPERIMENTAL RESULTS AND DISCUSSION

Distribution of time-averaged wall pressure at the design speed with medium loading.

Fig.4(a) shows velocity triangles at the rotor and the stator inlets obtained near the tip endwall at the design speed with medium loading. The incidences of both cascades here are negative with −45.2 deg for the rotor and −2.4 deg for the stator.

Fig.4(b) presents time-averaged distributions of the endwall pressures, CPw, in the rotor shown in the rotational frame of reference and in the downstream stator shown in the stationary frame. Note that both of the contour plots for the rotor and the stator are not connected to each other at their boundary in the case of time-averaged representations in different frames of reference. In both blade passages, large pressure gradient regions (indicated by LPG) are seen along the blade pressure surfaces of the downstream half of the passages. In these regions, the pressure drops significantly where the leakage flows enter the tip clearances with large flow acceleration around the pressure-side blade tip edges. Occurrence of this kind of pressure drop area has been already reported in stationary cascades (e.g. Bindon, 1986; Yamamoto, 1989), and now is seen also in the rotor.

Fig.4(c) shows distributions of the time-averaged random fluctuation of the pressure. Significantly large pressure fluctuations occur along both sides of the rotor blade and along the suction side of the stator blade. These areas with large random fluctuations indicated by LFp and LFs correspond to the inlet and the outlet of the leakage flow into or out of the tip clearance. Since the areas with large random fluctuation coincide precisely with high loss regions as seen later in Fig.10, it can be said that a large part of the endwall loss including the leakage loss generates and accumulates here where the leakage flow goes into and out of the clearance. The abrupt convergence and divergence of flow there cause the leakage loss. It may be interesting to see, in each cascade, that the contour plot of the time-averaged random fluctuation, $\overline{CPw'}$ has multiple maximum peaks along the surfaces of both blades, while that of the time-averaged pressure $\overline{CPw}$ has a single minimum peak.

Effect of rotor speed with different loadings.

(a) At decreased rotor speed with high loading.

Fig.5(a) shows velocity triangles near the tip endwall when the rotor speed is decreased to 330 rpm. As was seen in Table 2,

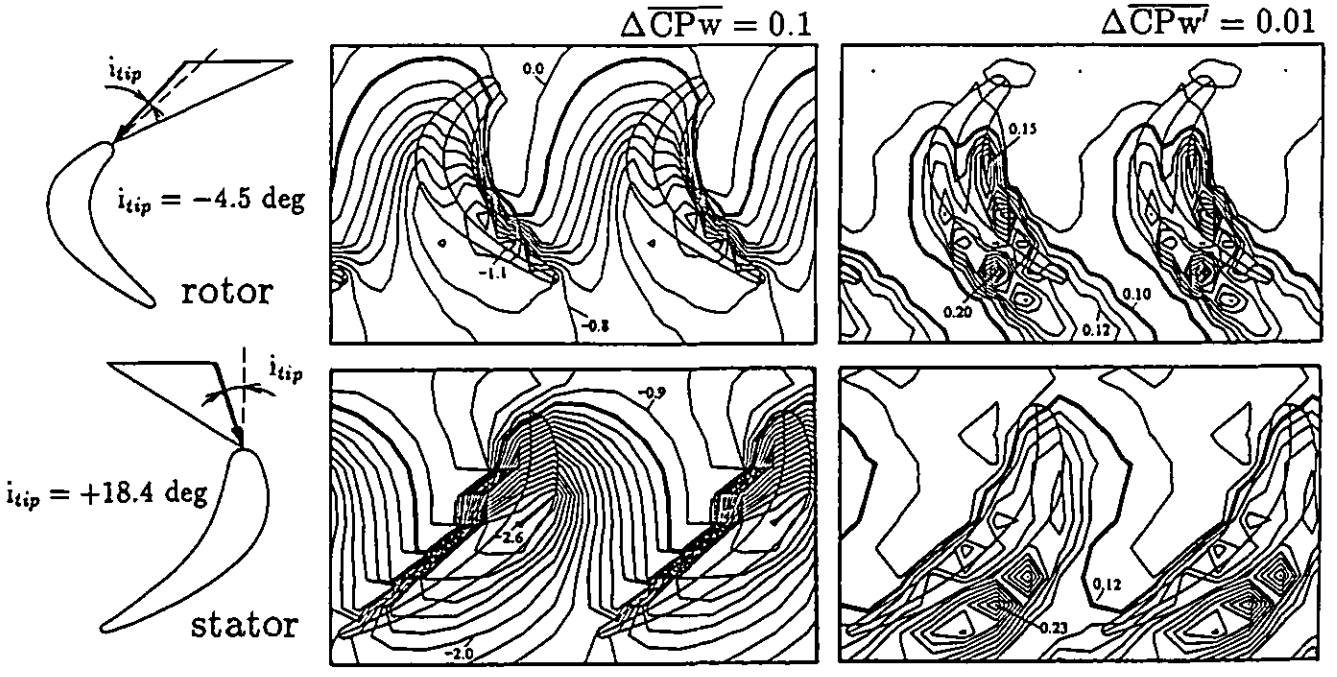

(a) velocity triangle at tip endwall

(b) endwall static pressure $\overline{CPw}$

(c) random fluctuation of endwall static presure, $\overline{CPw'}$

Fig.5 Time-averaged distributions at high loading

as the rotor speed is decreased with keeping the turbine mass flow rate constant, incidences of both the rotor and the stator at any spanwise locations tend to increase toward positive values and the flows tend to collide with the pressure sides of both blade leading edges. At this condition, turning angles of the flows through both blade passages become larger compared to those at the design speed, and the blade loadings become higher. The pressure differences between the pressure and the suction sides increase, so that the leakage flows are more accelerated as shown in Fig.5(b) with denser contours along the pressure surfaces than those seen in Fig.4(b). The areas with these large pressure gradients extend farther upstream, compared to those at the design speed, indicating that the velocities and, therefore, the mass flow rates of the leakage flows increase, and that the leakage flows begin to pass the clearances from farther upstream. It can be also seen in both rotor and stator that the locations of the minimum pressure peaks tend to enter the tip gaps at this high loading condition.

Fig.5(c) shows the time-averaged random fluctuations of the pressure. The areas with large fluctuation also extend farther upstream. This confirms, also in the present rotating blade row, that the leakage loss starts to generate from farther upstream as the blade loading increases, as was seen in a stationary cascade (Yamamoto, 1989).

(b) At increased rotor speed with low loading.

Fig.6(a) shows the velocity triangles at the rotor and the stator blade tips when the rotor speed is increased to 760 rpm. At this rotor speed, the incidences of both rotor and stator become large negative values. Turning angles of the flows through the cascades and accordingly, the blade loadings, decrease compared to those at the design speed.

Fig.6(b) shows the time-averaged pressure distributions where the area with large pressure gradient along the pressure surface of the 'rotor' blade has almost diminished, showing decrease of the leakage flow from this area. At this rotor speed, the cascade inlet flow collides with the blade suction side with large negative incidence, and the stagnation area of the cascade inlet flow moves to the suction side of each blade leading edge, as indicated by ST. The pressure gradient normal to the suction surface in the stagnation area increases, and therefore, some amount of leakage flow passes the tip clearance from the suction side to the pressure side. This leakage entering the gap from the 'suction' surface was seen also in the previous study (Yamamoto, 1989) done with a stationary linear cascade; some results are again presented in Fig.7 for two tip-side incidences of −24 and −62 deg (the corresponding midspan incidences are +7.2 and −53.3 deg, respectively). As the tip-side incidence changes from −24 to −62 deg, the endwall flow vectors in Fig.7(a) clearly

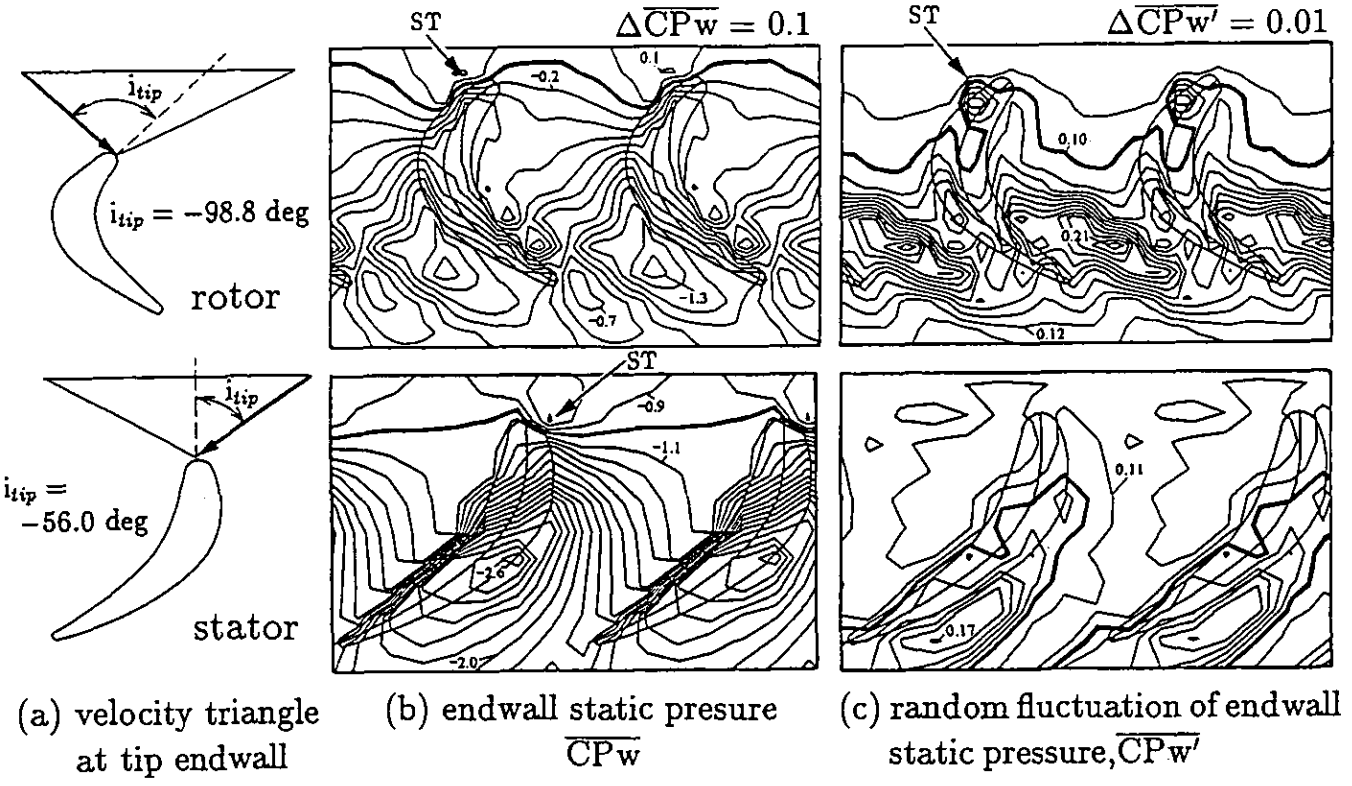

Fig.6 Time-averaged distributions at low loading

show that the leakage tends to enter the tip clearance from the suction side near the leading edge. The static pressures in Fig.7(b) also show that the large pressure gradient area seen along the pressure surface tends to disappear, but a new area with large pressure gradient appears along the blade suction surface near the leading edge.

In the downstream stator shown in Fig.6(b), however, the effect of the loading (or incidence) variation on the pressure field is not so significant as in the upstream rotor because of the larger leading edge radius of the stator and the smaller turning angle of flow.

Fig.6(c) shows the time-averaged random fluctuation of the endwall static pressure. In the rotor, large fluctuation occurs in the stagnation area (indicated by ST) which corresponds to the inlet of some amount of the leakage flow, and also in the downstream half of the rotor passage where the fluctuation spreads widely in the cascade circumferential direction. The latter fluctuation occurs in the following manner (see also Yamamoto, et al., 1994): (1) Since the inlet flow collides with the blade suction side of the leading edge with a fairly large negative incidence, the cascade inlet flow separates from the pressure side of the leading edge. (2) Low energy fluids generated by this separation, which are initially distributed in the blade spanwise direction over the blade pressure surface near the leading edge, are driven toward the tip or the hub endwalls by the tip- and hub-side passage vortices. (3) In the downstream half of the cascade passage, the low energy fluids cover the whole endwall during their migration toward the suction side of the rotor passage following the pressure gradient.

The low-energy fluids cause large random fluctuation in the endwall pressure, but as seen from Fig.6(c), effect of this large fluctuation does not extend downstream of the rotor, and the rotor-stator interaction, therefore, becomes weak. At this low loading, the peak value of the random fluctuation in the rotor stays at the same level as the other loading cases, while in the stator, it decreases. This reduction in the random fluctuation is resulted from the weaker rotor-stator interaction as well as weaker passage and leakage vortices occurring in the stator due to the reduction in the turning angle of the flow.

Time variation of endwall pressure due to rotor-stator interaction.

Fig.8(a) and (b) show time variations of the endwall pressure CPw and of the random fluctuation CPw' presented in the minimum periodical pitch width, i.e., five rotor pitch widths or four stator pitch widths.

The pressure distributions in the rotor shown in Fig.8(a) indicate that the time variation of the pressure caused by the rotor-stator interaction tends to decrease as the blade loading decreases with the rotor speed being increased. This tendency in the pressure variation in the downstream stator can be clearly

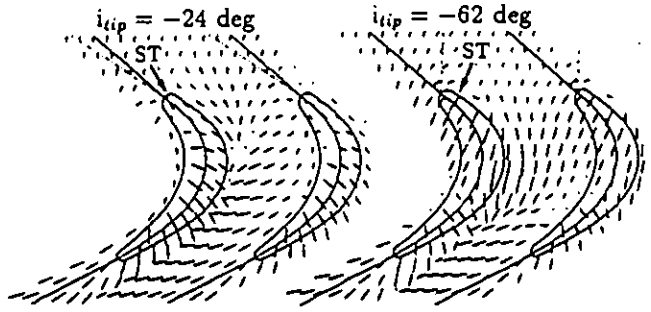

(a) endwall flow

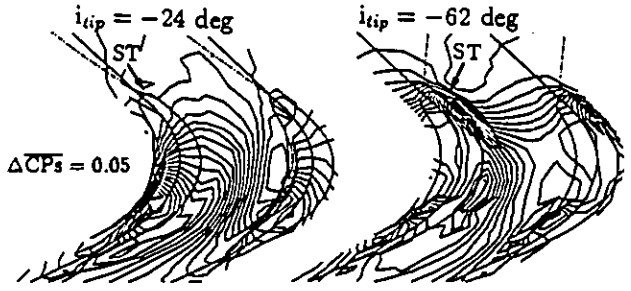

(b) static pressure near endwall

Fig.7 Tip leakage flow and static pressure near the endwall for two loadings (results from stationary linear cascade tests)

recognized by the periodic variation of the minimum pressure peak area shown with dark shades.

As shown in Fig.8(b), the random fluctuation along the blade 'pressure' surface generated by the leakage flow is affected by the rotor-stator interaction. The fluctuation along the suction surface, on the other hand, which is generated mainly by the passage vortex and the leakage vortex, also varies with time due to the rotor-stator interaction. Wakes of the upstream rotor with large fluctuations penetrate periodically and deeply into the downstream stator passage, as indicated by W, for example.

This is the case also for the free stream with smaller fluctuation as indicated by F. However, the large fluctuation does not extend far downstream at this low loading condition shown by the bottom figure in Fig.8(b) and does not affect the downstream stator cascade flow so significantly.

Relation between the random pressure fluctuation and the total pressure loss.

The present results were compared to some other test results separately obtained inside the rotor passage with five-hole Pitot tubes. Details of the measurements in the rotational frame of reference may be found in Yamamoto et al. (1994). Fig.9 compares the time-averaged endwall static pressure with the

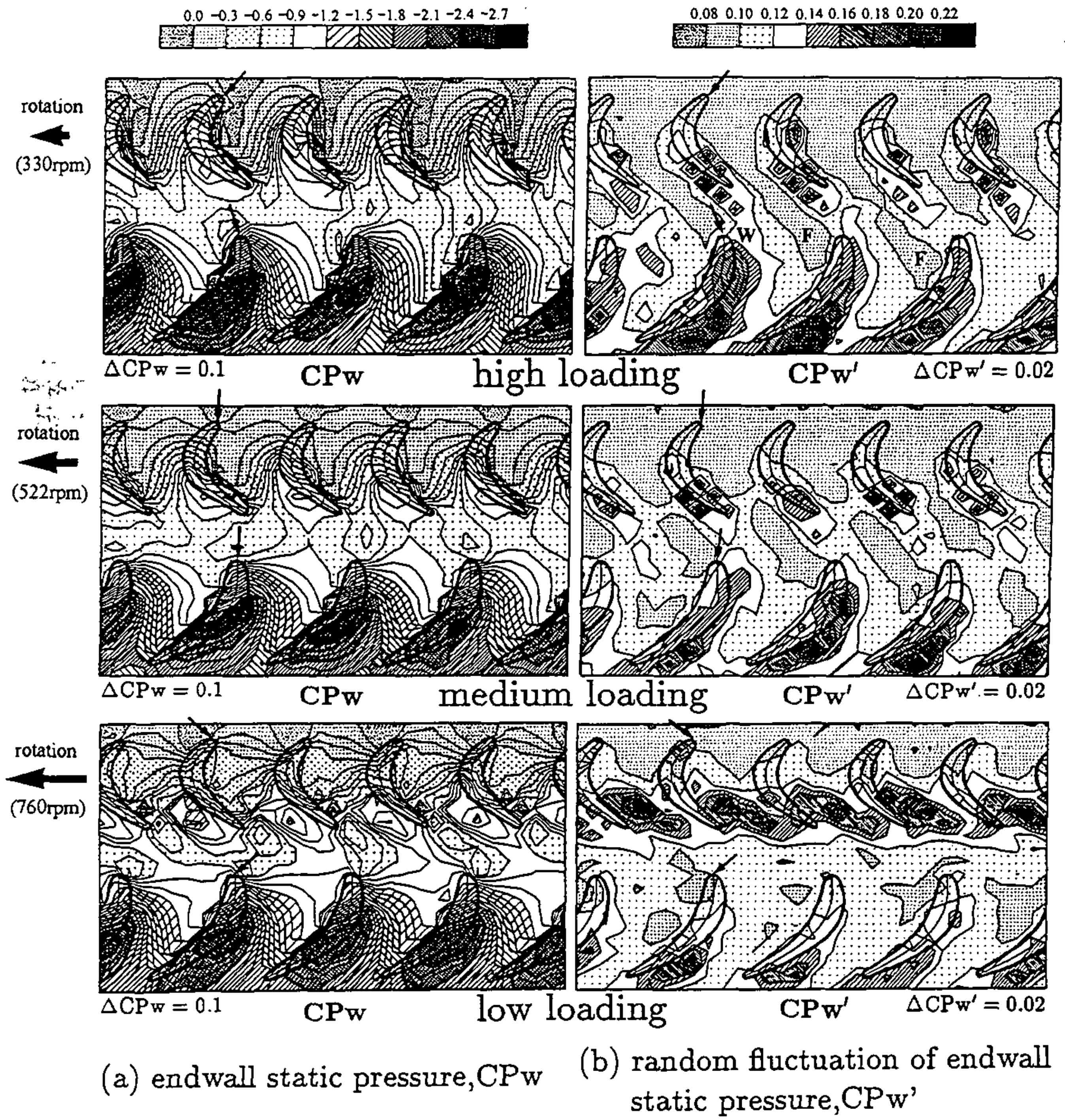

Fig.8 Effects of rotor-stator interaction on endwall static pressure and the random fluctuation

static pressure inside the rotor. The present three-dimensional representation of the static pressure inside the rotor passage and on the endwall pressure makes the origin of the cascade flow field be understood easily. A strong passage vortex exists near the hub endwall.

Fig.10 compares the time-averaged random fluctuation of the endwall pressure with the total pressure loss inside the rotor passage. It is interesting to know that both distributions of the random fluctuation and the total pressure loss surprisingly coincide with each other. This means that the unsteady behavior

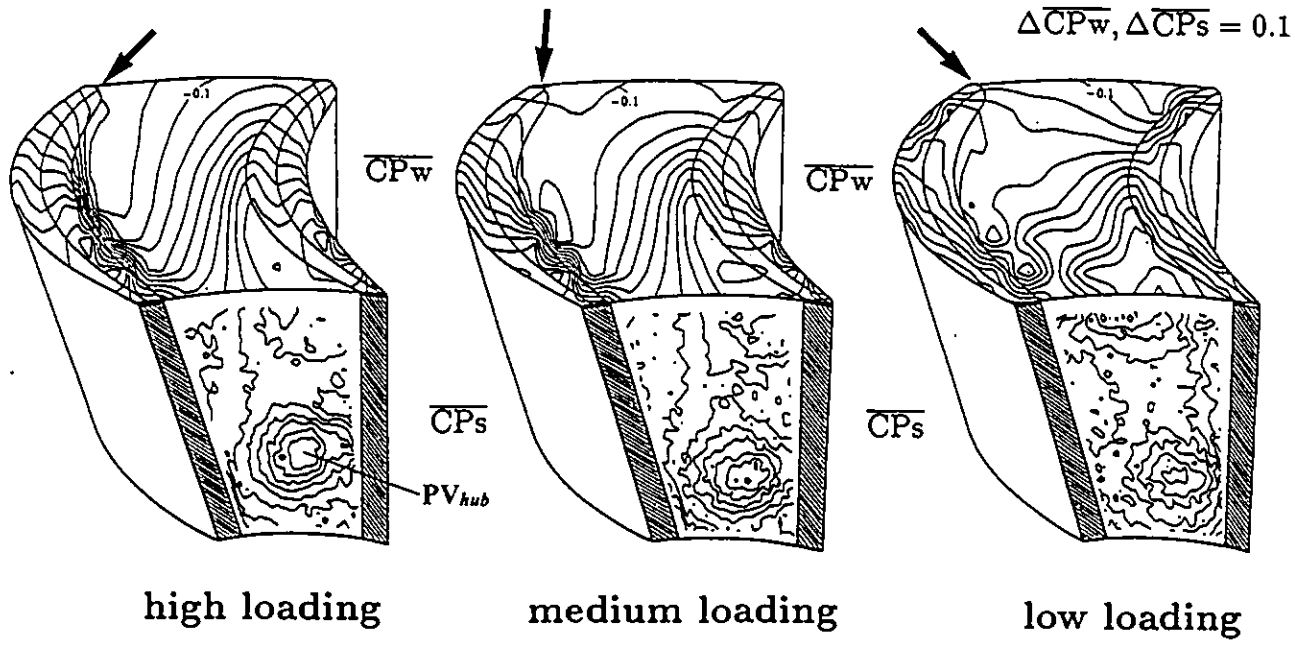

Fig.9 Time-averaged static pressure distributions on the rotor endwall and inside the rotor

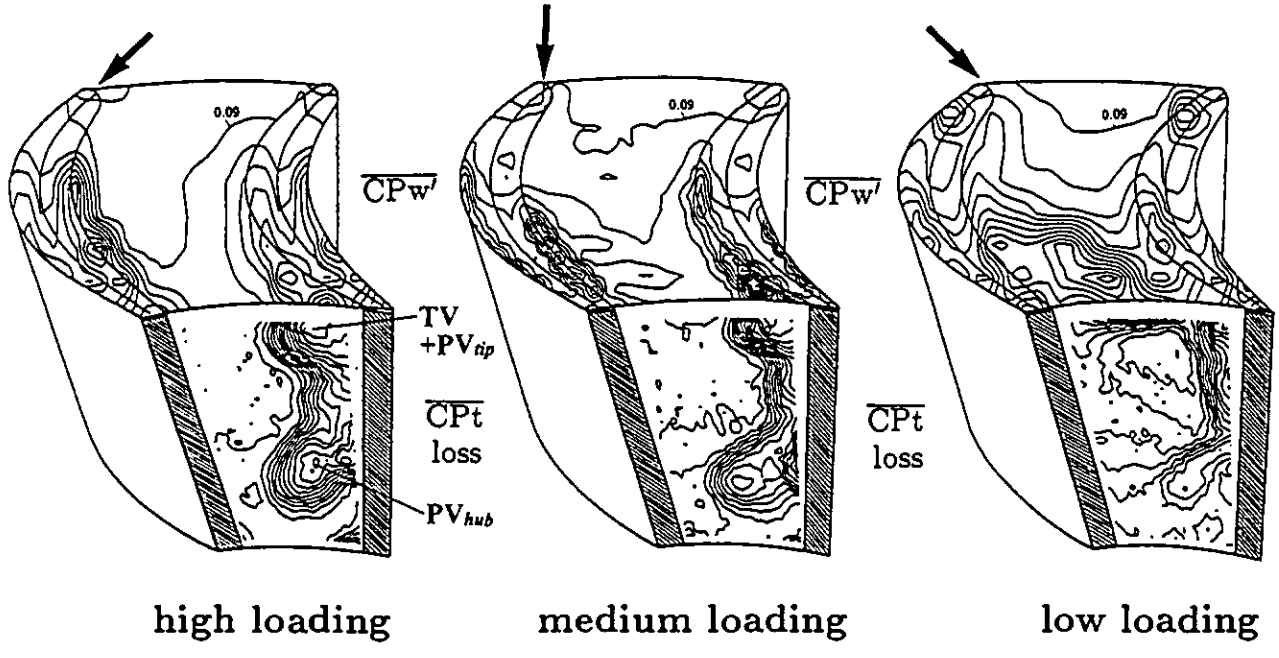

Fig.10 Comparison of time-averaged random fluctuation and total pressure loss inside rotor

of the total pressure loss can be known from that of the random fluctuations of the static pressure. At high and medium loadings, two loss cores exist on the blade suction surface. The cores were formed by the strong hub-side and weak tip-side passage vortices and the leakage vortex. At low loading, low-energy fluid generates from the flow separation at the leading edge and passes over the endwall toward the suction side, and finally migrates onto the blade suction surface. Thus, patterns of the unsteady loss generation processes could be seen through the unsteady behavior of the random fluctuation caused by the rotor-stator interaction.

CONCLUSIONS

1) It is confirmed, not only in the stator but also in the rotor, that large pressure drop occurs along the blade pressure surface where leakage flow enters the tip clearance.

2) The random fluctuation of the endwall pressure is large around the blade surface where the leakage flow enters and exits from the tip clearance. A large part of the leakage loss generates around the blade surface when the leakage flow abruptly converges and diverges there.

3) As the blade loading increases, the large pressure drop and the large random fluctuation start to generate from farther upstream in blade passages, which means that the leakage flow and the associated loss start to generate from farther upstream at higher loading.

4) At the test medium and high loadings, the rotor-stator interaction is strong since the random fluctuation generated from the upstream rotor penetrates deeply into the downstream stator passage.

5) As the blade loading decreases with large negative incidences, large random fluctuation occurs due to flow separation from the blade leading edge, and covers the whole endwall area in the downstream half of the rotor passage, leading the endwall loss to increase there. The random fluctuation, however, does not extend farther downstream, and the rotor-stator interaction is weak at this low loading with large negative incidences.

6) Rotor-stator interaction significantly affects the endwall flow and the leakage flow in both blade passages, and makes the loss generations unsteady.

7) The areas of large random fluctuation of static pressure coincide precisely with the areas of high total pressure loss.

REFERENCES

Bindon, J.P. 1986, "Pressure and Flow Field Measurements of Axial Turbine Tip Clearance Flow in a Linear Cascade," Cambridge University Engineering Department, Report No. CUED/A-Turbo TR 123.

Bindon, J.P., 1988, "The Measurement and Formation of Tip Clearance Loss," ASME paper 88-GT-203.

Heyes, F.J.G., Hodson, H.P., and Dailey, G.M., 1991, "The Effect of Blade Geometry on the Tip Leakage Flow in Axial Flow Turbine Cascades," ASME paper 91-GT-135.

Moore, J., and Tilton, J.S., 1987, "Tip Leakage Flow in a Linear Turbine Cascade, "ASME paper 87-GT-222.

Yamamoto, A., 1989, "Endwall Flow/loss Mechanisms in a Linear Turbine Cascade with Blade Tip Clearance, "Transaction of the ASME, Journal of Turbomachinery, Vol.111, No.3, pp.264-274.

Yamamoto, A., Tominaga, J., Tomihisa, S., Outa, E., and Matsuki, M., 1993, "Unsteady Three-Dimensional Flow Behavior due to Rotor-Stator Interaction in an Axial-Flow Turbine," ASME paper 93-GT-404.

Yamamoto, A., Tominaga, J., Matsunuma, T., and Outa, E., 1994, "Detailed Measurements of Three-Dimensional Flows and Losses inside an Axial Flow Turbine Rotor," to be presented at this conference.

Yaras, M. I., and Sjolander, S. A., 1991, "Effects of Simulated Rotation on Tip Leakage in a Planar Cascade of Turbine Blades," ASME paper 91-GT-127.